RSC Applied Interfaces

ROYAL SOCIETY OF CHEMISTRY

PAPER

View Article Online
View Journal | View Issue

Open Access Article. Published on 12 March 2024. Downloaded on 3/30/2026 8:14:33 AM.
This article is licensed under a Creative Commons Attribution 3.0 Unported Licence.

Check for updates

Cite this: *RSC Appl. Interfaces*, 2024, **1**, 600

Polyvinylpyrrolidone-mediated synthesis of ultra-stable gold nanoparticles in a nonaqueous choline chloride–urea deep eutectic solvent†

Raúl Ortega-Córdova, ‡[a] Kaori Sánchez-Carillo, ‡[b] Saúl Carrasco-Saavedra,[b] Gonzalo Ramírez-García,[b] María G. Pérez-García,[c] J. Félix Armando Soltero-Martínez[a] and Josué D. Mota-Morales *[b]

Received 21st December 2023,
Accepted 12th March 2024

DOI: 10.1039/d3lf00261f

rsc.li/RSCApplInter

This study investigates the role of polyvinylpyrrolidone (PVP) as a capping and stabilizing agent for the synthesis of gold nanoparticles (AuNPs) in a nonaqueous choline chloride–urea deep eutectic solvent (DES). AuNPs are obtained *via* chemical reduction, using L-ascorbic acid at 60 °C. Specifically, the effect of PVP's molecular weight (M_n of 10, 40, and 360 kDa) on the AuNP morphology, size, and colloidal stability is studied. The effect of the PVP's M_n on the resulting AuNPs is evaluated through UV-vis spectroscopy, *via* localized surface plasmon resonance (LSPR). Meanwhile, the morphology and size distribution of the nanoparticles are analyzed using electron microscopy. Our findings indicate the presence of spherical AuNPs with sizes ranging between 15 and 23 nm for PVP of 40 and 360 kDa (LSPR = 540 nm), irrespective of the media's viscosity. Notably, PVP of 40 kDa also produces luminescent gold clusters of *ca.* 2 nm size, the formation of which depends on the PVP's concentration. PVP of 10 kDa produces heterogeneous-sized particles due to a limited stabilization effect, while PVP of 360 kDa imposes difficulties in transferring to water. The most promising outcomes are observed with PVP of 40 kDa, as the nonaqueous colloids exhibit exceptional colloidal stability, even with drastic thermal changes. Finally, we introduce a proof of concept for dual strain-responsive and plasmonic eutectogels due to the DES' ionic conductivity and overall colloidal stability of PVP-capped AuNPs. This is achieved by immobilizing the gold colloids within gelatin-based eutectogels, showcasing potential for innovative applications in responsive transient and iontronic soft materials.

Introduction

Metallic nanoparticles such as gold nanoparticles (AuNPs) are of scientific and technological interest due to their unique optical, catalytic, and biological properties.[1,2] Their application in many sectors, such as biomedicine, drug-delivery systems, and analyte detection, is due to their tunable optical properties,[3,4] most notably the presence of localized surface plasmon resonance (LSPR). The LSPR phenomenon arises from the dipole oscillations of the free electrons on the nanoparticle's surface,[5] which gives the aqueous AuNP colloids their striking color. The LSPR can be fine-tuned by changing the shape, size, crystallinity, and structure of the nanoparticles and the nature of the stabilizing agents.[6,7]

Syntheses of such AuNPs have been extensively explored through bottom-up techniques, which, essentially, build nanomaterials atom-by-atom, providing fine control over their shape, crystallinity, metal composition, and surface chemistry.[8] One of the most crucial stages of nanoparticle formation by wet chemical reduction is the stabilization process of the metallic clusters formed during the earlier stages,[7,9] in which counteractive repulsive forces are introduced to avoid particle agglomeration.[10] Most syntheses of AuNPs in aqueous media require a stabilizing agent to provide said counteractive repulsive forces. Typical stabilizing agents consist of polymers, *e.g.*, polyvinyl alcohol (PVA), or surfactants such as cetyltrimethylammonium chloride/bromide (CTAC/CTAB).[11,12] Stabilizing compounds can also play the role of structure-directing agents for morphologies such as spheres, octahedrons, cubes, and prisms.[13,14] In seedless synthesis of AuNPs, the final morphologies result

[a] *Centro Universitario de Ciencias Exactas e Ingenierías, Universidad de Guadalajara, Guadalajara, Jalisco 44430, Mexico*
[b] *Centro de Física Aplicada y Tecnología Avanzada, Universidad Nacional Autónoma de México, Querétaro, QRO 76230 Mexico. E-mail: jmota@fata.unam.mx*
[c] *Centro Universitario de Tonalá, Universidad de Guadalajara, Tonalá, Jalisco, 45425, Mexico*

† Electronic supplementary information (ESI) available. See DOI: https://doi.org/10.1039/d3lf00261f

‡ Both authors contributed equally.

© 2024 The Author(s). Published by the Royal Society of Chemistry

Open Access Article. Published on 12 March 2024. Downloaded on 3/30/2026 8:14:33 AM.
This article is licensed under a Creative Commons Attribution 3.0 Unported Licence.

from the interplay of thermodynamic (*e.g.*, reduction potential) and kinetic parameters (*e.g.*, concentration, mass transport, temperature, and the involvement of external species).[15,16] Also, the media in which nanoparticles are synthesized can significantly influence their morphology, size and stability. Thus, a topic of interest to design new AuNPs is the development of nonaqueous gold colloids which present improved colloidal stability and extended operational conditions for processing into functional materials.[17–20]

In this regard, deep eutectic solvents (DESs) have emerged as a novel class of designer solvents with properties similar to ionic liquids, whose melting points are significantly lower compared to those of their constituents.[21] DESs, in general, are considered environmentally friendly and inexpensive green solvents of simple preparation in its pure state.[22] Specifically, type III DESs are mixtures of ammonium salts (*e.g.*, choline chloride) and hydrogen-bond donors (HBDs, *e.g.*, urea) that remain liquid upon the establishment of hydrogen-bonding interactions.[23]

DESs enable the efficient, safer, and environmentally benign preparation of nanomaterials with interesting properties.[24–27] They have the potential to revolutionize nanomanufacturing by opening new horizons for nanostructure control and stability. The synthesis of nanoparticles using DESs, coupled with their subsequent processing into advanced materials and nanostructures, represents a perfect combination of efficacy and sustainability. Due to the DESs' extended hydrogen-bonding network structure in the liquid state, ionic environment, and unusual electrostatic conditions,[25,28] they can promote the self-assembly and growth of gold micro and nanostructures by chemical reduction without the need for capping agents. In previous studies, urea–choline chloride (U–ChCl) DES was used to synthesize AuNPs of sizes between 2 and 10 nm through wet chemistry.[29] Similarly, anisotropic gold nanostructures have been synthesized in DESs (nonaqueous and hydrated), ranging from stars, snowflakes, and spiked-shaped nanostructures between 350 and 1100 nm.[25]

In order to design nanostructures with controlled size and morphology, the use of polymers as steric stabilizers has been extensively explored in aqueous media.[30] Polyvinylpyrrolidone (PVP) is one of the most commonly used polymeric stabilizers, due to its non-toxicity, amphiphilic character, and the presence of C═O, C–N and $-CH_2$ functional groups. It acts as a surface stabilizer, growth modifier, dispersant, and mild reducing agent[31] during the formation of AuNPs in aqueous media, resulting in particles with low polydispersity and sizes below 50 nm.[30] However, there are no previous systematic studies on the effect of PVP as a stabilizing agent on AuNPs in DESs, and the outcomes of its molecular weight on the synthesis of AuNPs in nonaqueous media such as DESs remain unexplored. This work sought to obtain AuNPs with controlled shape and size in a nonaqueous DES using PVP as a colloidal stabilizer. This is possible by exploiting the PVP's more flexible coil structure and open conformation when dissolved in a U–ChCl DES, compared with the more closed rod-like structure in water.[32] Hence, in this work we evaluated the effect of three different molecular weights of PVP, (10, 40 and 360 kDa) and its role as a stabilizing agent during the seedless synthesis of AuNPs in U–ChCl DES by chemical reduction using L-ascorbic acid at low temperature, *i.e.*, 60 °C. The exceptional thermal, and overall, stability of the nonaqueous gold colloids was demonstrated by immobilizing the PVP-capped AuNPs in a gelatin-based eutectogel (Fig. 1). The resulting plasmonic eutectogel was able to display both electrical conductivity and optical responses due to the AuNPs' LSPR.

Experimental section

Reagents and methods

Polyvinylpirrolidone (PVP) of different molecular weights (10, 40, and 360 kDa), chloroauric acid trihydrate ($HAuCl_4{\cdot}3H_2O$), L-ascorbic acid, choline chloride (98% purity), urea (99% purity) and type A gelatin (175 g Bloom) were purchased from Merck-Sigma Aldrich and used without any further purification.

DES preparation. Firstly, the choline chloride–urea DES was prepared by following previous procedures.[22] Briefly, a mixture of urea and choline chloride in a 2 : 1 molar ratio, respectively, was heated at 80 °C in an oil bath under constant stirring until a homogeneous liquid was formed. The mixture was left to cool at room temperature.

AuNP synthesis. 10 mL of $HAuCl_4{\cdot}3H_2O$ in DES (0.25 mM) was heated at 80 °C in an oil bath for 20 minutes, after which 0.125 g of PVP (1 wt% of DES + PVP) was added and left to dissolve under constant stirring until a homogeneous

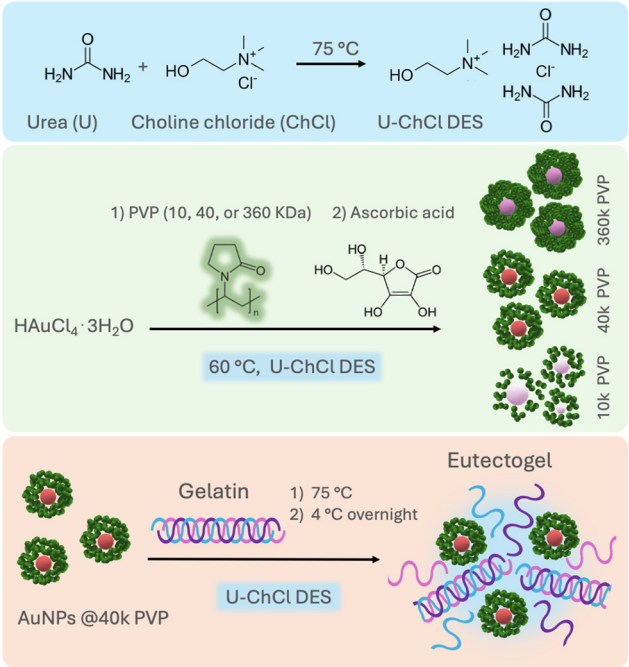

Fig. 1 General route for the synthesis of ultra-stable PVP-capped AuNPs in nonaqueous U–ChCl DES and preparation of plasmonic eutectogels.

Open Access Article. Published on 12 March 2024. Downloaded on 3/30/2026 8:14:33 AM. This article is licensed under a Creative Commons Attribution 3.0 Unported Licence.

solution was formed. The temperature was then reduced to 60 °C. Once the temperature had stabilized, 10 mL of L-ascorbic acid solution (0.2 mM) in the DES, previously heated at 60 °C, was added to the gold–PVP solution and left under constant stirring for 24 h in order to ensure that the nanoparticle formation reaction had reached its endpoint. The same procedure was followed for all samples, using PVP with different molar weights. Nanoparticles with 40 kDa PVP in water were also synthesized as a reference following the aforementioned methodology, and their characterization can be found in the ESI.†

Plasmonic eutectogel preparation. The eutectogel was prepared by following a previously reported protocol. Shortly, a 22 wt% gelatin solution was prepared using the obtained gold colloid suspension under slow stirring and heated up to 75 °C for 1 h until the gelatin was totally dissolved. The plasmonic eutectogel was then casted in a desired mold and left to gel at 4 °C for 24 hours.

Instrumentation

Optical characterization. The obtained gold colloids and the plasmonic eutectogel were analyzed through a UV-vis spectrophotometer (Genesys 840-208200, Thermo Scientific) in the 400–800 nm range, and using a choline chloride–urea DES as the blank. Cylindrical and rectangular stretched and relaxed samples of the plasmonic eutectogel were attached to the side of a quartz cuvette.

The hydrodynamic radius in DES was measured through dynamic light scattering (DLS) using a Malvern equipment model ZSIZER90 considering the DES viscosity as: 115 mPa s.

For electron microscopy and energy dispersive spectroscopy (EDS) analyses, a HITACHI SU8230 cold cathode field emission scanning electron microscope and a JEOL JEM1010 transmission electron microscope were used.

The attenuated total reflectance-Fourier transform infrared (ATR-FTIR) characterization of AuNPs precipitated from the DES was performed using an IR spectrophotometer (Perkin Elmer, Spectrum Two). X-ray photoelectron spectroscopy (XPS) data were obtained using an XR50M monochromatic Al Kα ($h\nu$ = 1486.7 eV) X-ray source and a Phoibos 150 spectrometer with a one-dimensional ID-DLD detector provided by SPECS. PVP-capped AuNPs in DES were washed with water in a 1 : 3 volume ratio and separated through centrifugation at 1200 rpm for 20 min. This procedure was repeated 4 times to remove the DES. Then, the samples were mounted on a silicon plate and dried in a convection oven at 70 °C. The peak-fitting analysis was made by employing the AAnalyzer software. The energy axis of all measurements was corrected for potential energy shifts by aligning the position of the maximum of the C 1s photoemission peak with the C–C/C–H carbon atoms of the PVP at 285 eV.

Plasmonic eutectogel characterization. A universal testing machine (Z005, Zwick-Roell) was used on the cylindrical samples (20 mm diameter × 4.6 mm thickness) to evaluate the compression performance of the eutectogel at 50% of their maximum compressive strain at room temperature. The evaluation of the thermal properties of the eutectogel was performed by differential scanning calorimetry (DSC-250, TA Instruments). Scans were carried out at 1 °C min^{-1} under a nitrogen flow. The plasmonic eutectogel was firstly cooled to −20 °C and kept at that temperature for 10 minutes before heating up to 120 °C and cooling down to RT. The U–ChCl DES was firstly cooled to −60 °C and kept at that temperature for 5 minutes before heating up to 90 °C and cooling down to RT. In order to measure the sensitivity of the eutectogels, the gauge factor (GF) was calculated as the change in the resistance of the sample when stretched. The GF was measured using a USB digital multimeter (SPRKC-TOL-12967, Sparkfun) and calculated according to the following equation:

$$\mathrm{GF} = (\Delta R/R_0)(\Delta L/L_0) \quad (1)$$

where ΔR represents the electrical resistance at a selected strain, R_0 represents the initial electrical resistance, and $\Delta L/L_0$ is the relative strain.

Results and discussion

Nanoparticles in DES

The effect of PVP's M_n on the synthesis of AuNPs was first evaluated using L-ascorbic acid as the reducing agent for $HAuCl_4{\cdot}3H_2O$ at 60 °C in the archetype DES composed of choline chloride and urea in a molar ratio of 1 : 2, respectively. The concentrations of the gold precursor (0.25 mM), reducing agent (1 mM, 4 : 1 molar ratio to the Au precursor), and PVP (1% wt) in the reaction mixture were chosen based on previous reports on the synthesis of spherical AuNPs in water.[33,34] Moreover, in this work, we aimed to lower the precursor's concentration compared to that used in previous reports on AuNP syntheses in U–ChCl DES (*ca.* 10–20 mM).[35] These figures provide a starting point for comparing the behavior of PVP in DES against a well-known aqueous system for AuNP synthesis.

Fig. 2 shows a digital photograph of the coloration obtained at the endpoint of each synthesis using PVP of different M_n: 10, 40, and 360 kDa, hereafter referred to as 10 k PVP, 40 k PVP, and 360 k PVP, respectively. The resulting colloids exhibit distinctive colors depending on the PVP's M_n. This color shift results from changes in the LSPR of the nanoparticles, as evidenced in the corresponding UV-vis absorption spectra. The highest absorbance is observed for nanoparticles synthesized with 40 k PVP, showing a single narrow LSPR centered at 540 nm (FWHM = 64.6 nm) (Fig. S1†). In water, this band is associated with spherical morphology and low polydispersity.[36] Similarly, the LSPR of the AuNPs stabilized with 360 k PVP shows a slight blue shift and lower intensity (LSPR = 535 nm; FWHM = 64.6 nm), suggesting spherical nanoparticles of similar size. However, the AuNPs obtained with 10 k PVP exhibit two absorption bands, the first at around 530 nm (FWHM = 40.6 nm) and a

 © 2024 The Author(s). Published by the Royal Society of Chemistry

Open Access Article. Published on 12 March 2024. Downloaded on 3/30/2026 8:14:33 AM.
This article is licensed under a Creative Commons Attribution 3.0 Unported Licence.

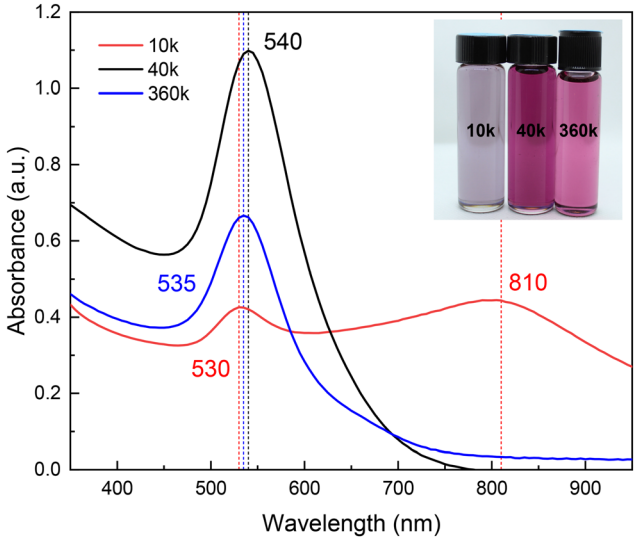

Fig. 2 UV-vis absorption spectra of the synthesized AuNPs in U–ChCl DES capped with different molecular weights of PVP. The inset shows a digital photograph of these colloids.

second one at around 810 nm (FWHM = 131.2 nm). The width of those bands also implies high polydispersity (Fig. 2). These results are similar to those obtained by Hussain, *et al.*[34] who synthesized AuNPs in a water–ethanol mixture by reducing 5 mM $HAuCl_4$ with L-ascorbic acid using PVP as a stabilizing agent. Their results show a single plasmon band at around 520 nm, which shifted to longer wavelengths with increasing ethanol content. These nanoparticles exhibited sizes ranging from 22 to 28 nm, which is similar to the present study.

To evaluate the impact of the solvent on the syntheses, AuNPs were also prepared in water, maintaining all other parameters. The resulting colloids in DES exhibited light purple (10 k PVP), bright pink (40 k PVP), and light pink (360 k PVP) colors, in contrast to the bright red color of the AuNPs obtained with 40 k PVP in water (Fig. S2†). It is possible that the observed red shift in the AuNP plasmon in DES compared to those in water is due to larger particles sizes. Electronic microscopy results revealed that particles in DES were, in fact, of larger sizes than those in water (Fig. S3†), approximately 20 and 10 nm, respectively. In addition, the physicochemical properties of the DES, such as the refractive index and AuNP concentration, are partly responsible for the observed optical differences.[37]

Steric stabilization is a process wherein colloidal particles are prevented from aggregating through adsorption of large molecules onto the particle surface, forming a protective layer.[10] The presence of large molecules, such as PVP chains, in the interparticle space would result in a polymeric barrier.[10,38] This barrier envelops individual nanoparticles with a preserving layer of a long solvate polymer, a phenomenon accentuated within the non-volatile DES.[32] It is, therefore, reasonable to assume that the molecular weight of the polymer chains as a steric stabilizer directly influences the effectiveness of AuNPs in the DES. As indicated by the presence of two plasmons (Fig. 2), the AuNPs synthesized with 10 k PVP are not stable, due to the chain length of the PVP being too short to provide long-term steric stabilization.[39]

PVP-capped AuNPs were observed through electron microscopies after precipitation from the DES with water. The effects of PVP-mediated steric stabilization on AuNPs are evident in the TEM and STEM micrographs, being directly linked to particle size, coalescence, and M_n, as will be discussed further. As shown in Fig. 3a, for 10 k PVP, individual spherical particles of 24.4 ± 12.8 nm average (mode = 15.9 nm) are responsible for the wide LSPR at 530 nm as shown in Fig. 2. Larger agglomerates of those particles could be associated with the plasmon at 810 nm (Fig. S4†). In addition, there is a second population with sizes between 40 and 60 nm. These results show that the barrier formed by the low molecular weight PVP is unable to effectively control the nanoparticle size and prevent their aggregation. In contrast, the AuNPs synthesized with 360 k PVP (Fig. 3b) present a single population of AuNPs with an overall size of 18.5 ± 5.2 nm and quasi-spherical shape within polymer residues. Despite the homogeneous particle size that could be attributed to the polymer's larger molecular weight, washing the polymer away proved to be a challenge when transferred to water. This could be detrimental to further applications that require different surface functionalizations.[28,38,40] Similar results for the AuNP size were obtained for 40 k PVP (Fig. 3c). These AuNPs also exhibit quasi-spherical morphologies, a narrower size distribution of 21.3 ± 4.1 nm and high stability under ambient conditions for up to 6 months (Fig. S5†), consistent with the observed UV-vis absorption spectra reported in Fig. 2. The results demonstrate that the PVP with a M_n of 40 kDa is optimal to provide a steric barrier for the plasmonic AuNPs during their synthesis and as a stabilizing agent for the final nonaqueous colloids in the DES.

To study the AuNPs synthesized with 40 k PVP, TEM was performed on the precipitated particles from the DES and DLS of the as-synthesized colloids in the DES. The hydrodynamic radius obtained in DLS (26.9 nm), measured directly in DES, is larger than the particle size observed by TEM (21.3 nm), which agrees with the literature, as DLS has higher sensitivity for bigger particles and also takes into consideration the capping PVP.[41] Precipitated PVP-capped AuNPs were also analyzed through XPS and EDS. The high-resolution spectrum of the gold 4f core level and EDS analysis confirmed the presence of metallic gold. FTIR, XPS and EDS also revealed the expected functional groups resulting from the PVP capping agent and DES, namely, carbonyl, amino, ammonium, and chloride groups (Fig. S6†). Additionally, TEM images and DLS results show an additional population of smaller particles of *ca.* 2 and 11 nm, respectively, which will be discussed in detail below.

To gain deeper insights into the AuNP formation and growth, and the role of PVP as a capping agent, the LSPR was followed over time by UV-vis using the polymer with the M_n

Open Access Article. Published on 12 March 2024. Downloaded on 3/30/2026 8:14:33 AM.
This article is licensed under a Creative Commons Attribution 3.0 Unported Licence.

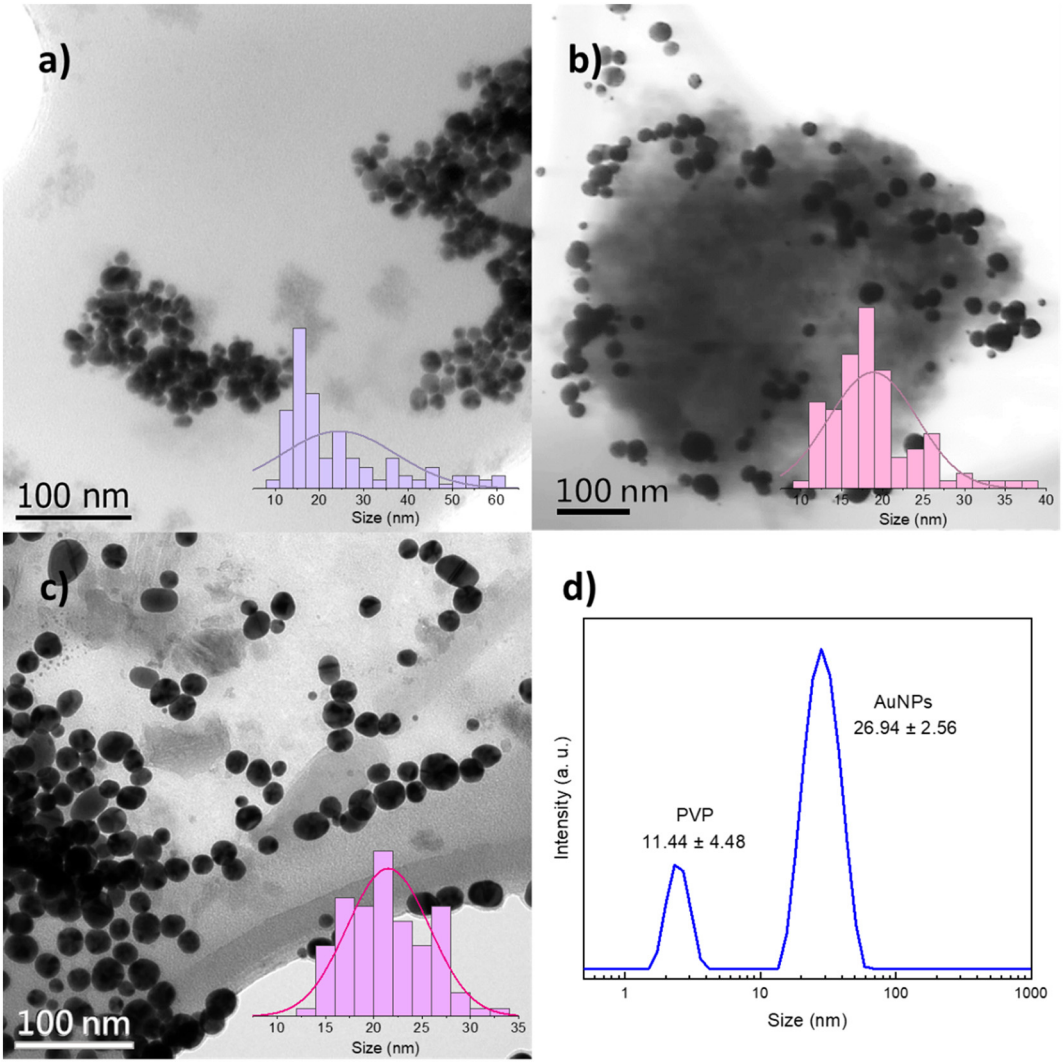

Fig. 3 TEM and STEM micrographs and particle size distribution histograms of the synthesized AuNPs with (a) 10 k PVP, (b) 360 k PVP and (c) 40 k PVP. (d) DLS hydrodynamic radius size distribution.

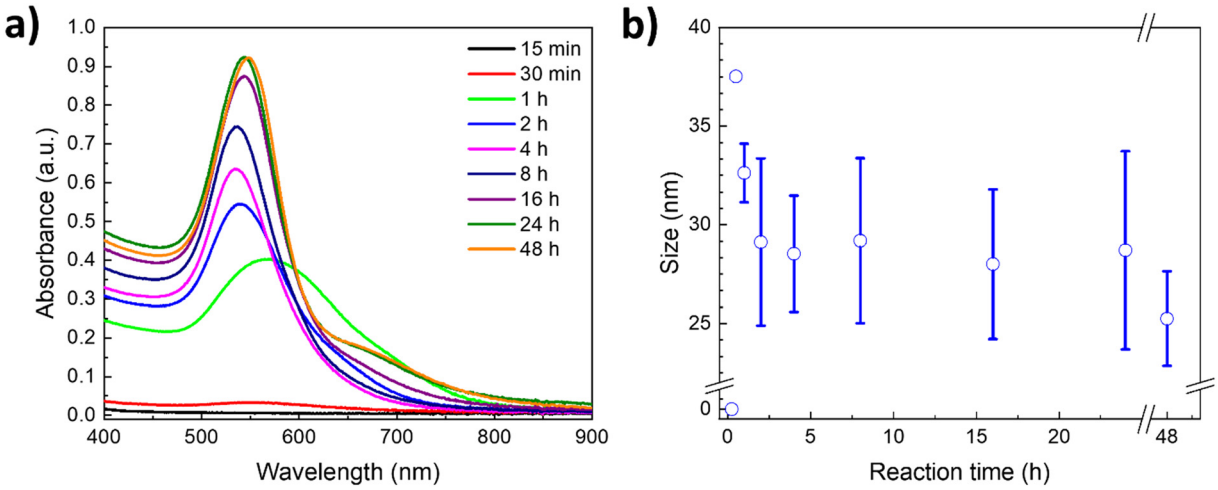

Fig. 4 (a) Kinetic study on the formation and (b) particle size of gold nanoparticles with their standard deviations as a function of reaction time, stabilized with 40 k PVP in a choline chloride–urea DES. Measurements were performed through UV-vis absorption spectroscopy and the DLS technique, respectively.

 © 2024 The Author(s). Published by the Royal Society of Chemistry

Open Access Article. Published on 12 March 2024. Downloaded on 3/30/2026 8:14:33 AM.
This article is licensed under a Creative Commons Attribution 3.0 Unported Licence.

of 40 kDa. Fig. 4a shows the corresponding kinetic study in a U–ChCl DES at 60 °C using L-ascorbic acid as the reducing agent. As can be appreciated, the reaction endpoint, *i.e.*, no changes in the LSPR intensity, is reached at 24 h, whereas the formation of plasmonic AuNPs starts at around 30 minutes after adding L-ascorbic acid to the PVP–gold solution in DES (LSPR = 565 nm).

A red-shift of the plasmon is observed during the first hour of the synthesis, which is due to the interactions of the gold precursor and other molecules with the particle surface,[10,42] including the DES components.[29,43,44] A digital photography of the nanoparticles' coloration shift throughout the reaction can be found in the ESI† (Fig. S7). According to Polte *et al.*,[10] the formation of nanoparticles in aqueous solution starts with a high reduction rate shortly after adding the reducing agent; this increases the number of particles, rapidly forming small zerovalent clusters. During the second phase, reduction continues while the unstable freshly formed particles undergo a coalescence process. Once the particles reach a stable mean size, the number of particles formed remains the same while their size continues to increase. Subsequently, particles grow due to the diffusion of reduced gold ions in the solution. Finally, the growth rate increases drastically, and the remaining gold salt is reduced rapidly.

This four-step synthesis mechanism is consistent with the UV-vis absorption spectra obtained for the kinetic study of AuNP formation in a nonaqueous DES. As such, during the first 15 minutes of the reaction (Fig. 4a) there is no observable plasmon, as the reduction of the gold precursor leads to the formation of non-plasmonic clusters; this is the first step. At 30 minutes, the reduction of the precursor is still ongoing, albeit a small plasmon can already be appreciated, resulting from the first plasmonic nanoparticles formed, suggesting that the second phase is taking place. The number of particles increases exponentially after that, as can be seen in the 1 hour measurement; this is the third phase. Afterwards, particles keep growing and stabilizing, until they reach stability at 24 hours, seeing no major change even at 48 hours of reaction. Furthermore, the relative increase in size of the nanoparticles after the third hour can also be appreciated, following the plasmon's location. The LSPR progressively shifts over time from around 533 nm to its final location at 543 nm, as the number of particles formed increased, associated with the intensity of the plasmon.

Simultaneous to the kinetic study through UV-vis spectroscopy, DLS measurements of each data point were performed, and the hydrodynamic radius results are presented in Fig. 4b. As can be appreciated, the size and standard deviation of the nanoparticles are consistent with the LSPR behavior observed through UV-vis spectroscopy. During the first hour of the synthesis, the particles show narrower size distribution, whereas at longer times the particles reach their final average size (*ca.* 20 nm, Fig. 4b) and the standard deviation becomes more prominent. This is a result of the increase in the concentration of plasmonic nanoparticles as deduced from the steady increase of the LSPR intensity (Fig. 4a).

Furthermore, the synthesized nanoparticles in DES exhibited great stability, showing no sign of agglomeration up to six months at room temperature after their synthesis. This high stability was also observed after subjecting the colloids to extreme thermal changes, centrifugation (10 000 rpm, 10 min) and sunlight exposure (Fig. S8†). For instance, 40 k PVP nanoparticles were frozen at −15 °C overnight (with evident solidification of the colloid) and then left to melt at room temperature, after which UV-vis absorption measurements were performed. Similarly, to evaluate the particles' stability at high temperatures, another sample of AuNPs was heated up to 90 °C for *ca.* 15 min and then left to cool at room temperature before measuring the UV-vis spectra. As can be observed in the obtained UV-vis absorption spectra in Fig. 5, there are no significant changes in the plasmon's width, intensity and wavelength. It can be concluded that the AuNPs synthesized in DES using 40 k PVP are highly stable in a wide range of temperatures; these temperature changes in water conduce to AuNPs agglomeration (Fig. S8†). This stability is likely a result of the intermolecular interactions of DES's components with PVP, mainly H-bonding, which prevent the agglomeration of the nanoparticles.[30]

To gain a deeper understanding of the PVP's behavior in DES and its role during the AuNP synthesis, the rheological properties of the PVP solutions in DES, with different M_n, were studied. On that note, viscosity measurements of the PVP solutions in DES were performed to explain the mass transport differences in the reaction media and to elucidate the origin of different AuNP average sizes and size distributions. Fig. 6a shows the viscosity of the 40 k PVP solution at 1 wt% at various temperatures (25, 45 and 60 °C) in a nonaqueous U–ChCl DES. It can be appreciated that the solution's viscosity is not affected by the shear velocity, indicating a Newtonian behavior for this

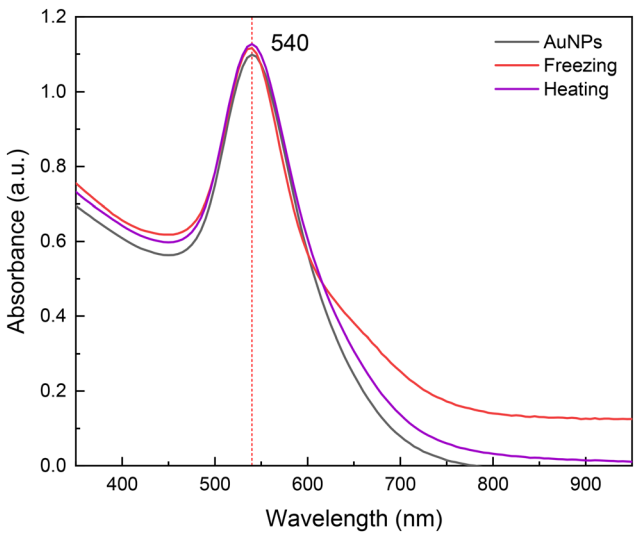

Fig. 5 UV-vis absorption spectra for gold nanoparticles stabilized with 40 k PVP (black), and after freezing and heating at −15 (red) and 90 °C (purple), respectively.

Open Access Article. Published on 12 March 2024. Downloaded on 3/30/2026 8:14:33 AM.
This article is licensed under a Creative Commons Attribution 3.0 Unported Licence.

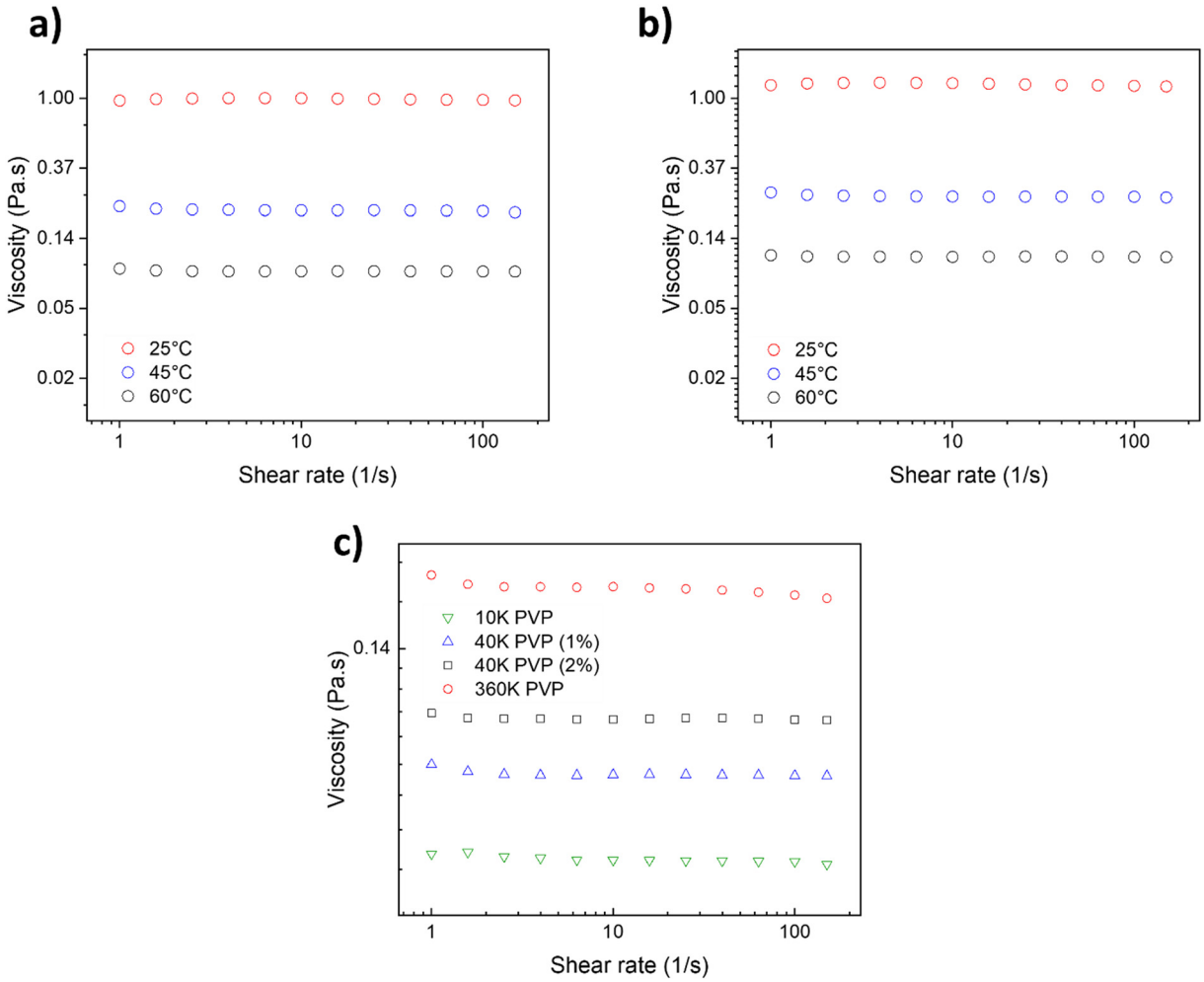

Fig. 6 Shear rate sweep of 40 k PVP at 1 wt% (a) and 2 wt% (b) at different temperatures and (c) a comparison of the viscosity of PVP with different molecular weights at 1 wt% for 10 k PVP, 40 k PVP and 360 k PVP and 2 wt% for 40 k PVP, at 60 °C.

concentration between 1 and 100 s^{-1}. This behavior is similar to that reported by Mjalli *et al.* for pure U–ChCl DES.[45] The viscosity of 1 wt% 40 k PVP in the U–ChCl DES is 89 mPa s at 60 °C, the temperature at which the nanoparticles were synthesized in this work. On the other hand, when the polymer's concentration was increased to 2 wt% (Fig. 6b), there was an increase in viscosity at 60 °C to 106 mPa s, also presenting a Newtonian behavior. As expected, the viscosity of the suspensions increased as the molecular weight of PVP (1 wt%) increased, with values of 72, 89 and 182 mPa s for 10, 40 and 360 kDa, respectively for measurements at 60 °C (Fig. 6c).

According to the results obtained from the synthesis of AuNPs, the viscosity of 1 wt% 40 k PVP was found to be optimal to the formation of AuNPs, in order to maintain a lower reaction rate and promote the formation of monodisperse and well-defined nanoparticles. It is well-known that viscosity and other properties directly impact the nanoparticle formation since they lead to a moderation of the reaction rate, allowing the metallic ions in solution to homogeneously nucleate and grow.[46]

The maximum solubility of 40 k PVP in the U–ChCl DES was found to be 5 wt%, where it produced an extremely viscous liquid at 60 °C (*ca.* 200 cP); these data are consistent with those reported by Sapir *et al.*[32]

As the physicochemical properties of the media strongly influence the particle formation phenomenon, we evaluated the effect of an increase in PVP concentration, keeping all other parameters constant, *e.g.*, concentration of the gold precursor and ascorbic acid, temperature, and reaction time. Fig. 7a presents the UV-vis absorption spectra of the AuNPs synthesized with increasing 40 k PVP concentration two-fold and four-fold (2 and 4 wt%); these values are below the solubilization limit. As can be seen from the spectra and the digital photograph, the LSPR slightly shifts with increasing PVP content from 540 nm to 538 nm, which does not suggest a significant change in the size of the AuNPs but suggests a change in the plasmon intensity (higher absorbance). This can be attributed to a significant increase of the plasmonic nanoparticle concentration in the colloid. To investigate the origin of such a significant increase in the plasmonic AuNP concentration with increasing PVP content, the colloids were

 © 2024 The Author(s). Published by the Royal Society of Chemistry

Open Access Article. Published on 12 March 2024. Downloaded on 3/30/2026 8:14:33 AM.
This article is licensed under a Creative Commons Attribution 3.0 Unported Licence.

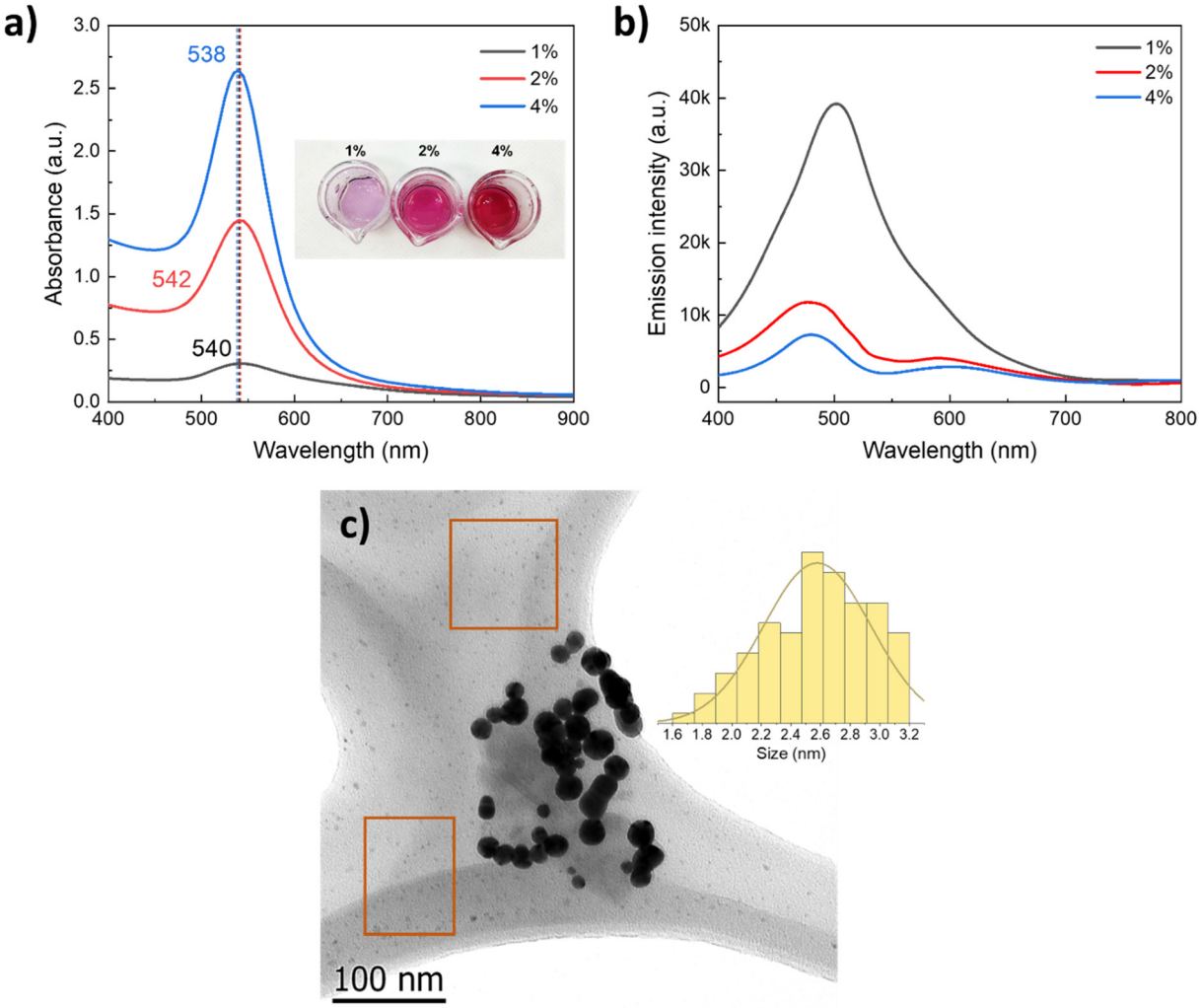

Fig. 7 (a) UV-vis absorption spectra for the AuNPs synthesized with various %wt (1, 2, and 4%) of PVP and a digital photograph of the diluted nanoparticles' coloration, (b) emission spectra of the AuNPs synthesized with different %wt of PVP after being excited with a 390 nm laser and (c) TEM micrograph of 40 k AuNPs surrounded by luminescent clusters (orange rectangles) with the clusters' size distribution histogram.

analyzed by fluorescence spectroscopy. The as-obtained colloids were excited with a UV laser (λ_{exc} = 390 nm), and the emission spectra were recorded. As reported for thiol-capped Au clusters of *ca.* 2 nm size in water, the sample with 1 wt% 40 k PVP presented a prominent emission peak centered at 510 nm,[47] corresponding to the emission of small luminescent gold clusters of <5 nm size.[48] The intensity of the emission due to the population of small Au clusters significantly decreased as the concentration of PVP increased, which is opposite to the intensity of the LSPR of plasmonic nanoparticles recorded by UV-vis (Fig. 7). This behavior points to the presence of a significant enough population of small Au clusters of 2.6 ± 0.4 nm size responsible for the luminescence. These Au clusters were observed in the background of the TEM micrographs of the AuNPs synthesized in the presence of 40 k PVP (Fig. 7c, orange squares) along with the plasmonic nanoparticles of 21.3 nm size (LSPR = 540 nm). Formation of these Au clusters was prevented by increasing the PVP concentration likely due to the involvement of PVP as not only the capping and stabilizing agent but also as a mild reductor that facilitates the growth of these Au small clusters into plasmonic AuNPs of *ca.* 20 nm size.[49]

Nanoparticles transferred to water

To study the behavior of the nanoparticles in aqueous media, the synthesized nanoparticles in DES were subjected to three washing steps and centrifuged at 6000 RPM for 15 minutes at RT. The pellet was recuperated and redispersed in water. After that, dynamic light scattering (DLS) and nanoparticle tracking analysis (NTA) measurements were performed. From the obtained results for both techniques, a significant increase in the nanoparticles' hydrodynamic radius in water is evident, compared to the results obtained for the same particles in DES (Fig. S9†). This can be attributed to the polymer's swelling in the presence of water as was extensively studied before.[32]

Open Access Article. Published on 12 March 2024. Downloaded on 3/30/2026 8:14:33 AM.
This article is licensed under a Creative Commons Attribution 3.0 Unported Licence.

In Fig. S9a,† the results for DLS measurements are shown; the mean sizes, obtained from the average of all populations, for the PVP-capped AuNPs in water were 672, 52.5 and 126 nm for 10 k, 40 k and 360 k PVP, respectively. It is worth noting that all samples present two main size distributions. The ones at lower values can be associated with the gyration radius of the polymer that corresponds to the M_n, 40 k and 360 k PVP,[50] and small AuNPs. For the 10 k sample, there is a contribution from both the polymer and smaller particles at lower sizes, whereas the second distribution can be associated with the presence of the agglomeration of the nanoparticles. This is consistent with the data obtained through UV-vis absorption spectroscopy (Fig. 2), where the nanoparticle size distribution decreased as the polymer's molecular weight increased. There is a significant increase in the hydrodynamic radius for all samples, in comparison to the measurements obtained for 40 k AuNPs in DES (Fig. 3d). Furthermore, the particles synthesized with 40 k PVP have the lowest polydispersity index of 0.324, which was obtained directly from the equipment, pointing to the effective capping of 40 k PVP, in contrast with 0.599 for 10 k PVP and 0.332 for 360 k PVP. According to the ISO standards (ISO-22,412:2017 and ISO-22,412:2017), nanoparticles with a polydispersity index above 0.7 are considered highly polydispersed; hence, the nanoparticles synthesized in this work are samples with low polydispersity.[51]

Similar results to those obtained here are those reported by Bandulasena *et al.*[39] who synthesized AuNPs in water in a capillary microfluidic device, using ascorbic acid as a reducing agent and PVP (1% w/v) of three molecular weights (10 k, 40 k, and 360 k PVP) as capping agents. Nanoparticles were measured with DLS and the results show sizes of 56–62 nm for 10 kDa, 72–92 nm for 40 kDa and 180–290 nm for 360 kDa. They also observed that the size of AuNPs decreases with the increase in ascorbic acid concentration. According to their results, nanoparticles synthesized with 40 k PVP show higher uniformity and monodispersity, whereas nanoparticles synthesized with other molecular weights present larger sizes and higher polydispersity that increases over time. These results are similar to those reported here. Nevertheless, their obtained particles for 360 k PVP greatly differ in size compared to the AuNPs synthesized in this work for that molecular weight; also, the reported sizes for 10 k PVP are significantly smaller. These discrepancies are likely a result of the PVP's more open conformation in the U–ChCl DES, allowing the formation of smaller particles in the case of 360 k PVP.

On the other hand, for NTA measurements, shown in Fig. S9b,† the mean sizes were 172.5, 75.7 and 132.2 nm for 10 k, 40 k and 360 k PVP, respectively. The behavior of the results is consistent with that observed through DLS and UV-vis absorption spectroscopy. However, measured sizes for 10 k and 360 k PVP were significantly different between NTA and DLS, being more notorious for 10 k PVP. This behavior is a result of the technique. DLS presents higher sensitivity for larger particles since it evaluates and compares the intensity of the light scattered by the particles, whereas NTA is based on the individual tracking of particles and the analysis of the speed at which they move as a result from their Brownian motion. This results in wider size distributions for NTA measurements, as is the case for the agglomeration of the AuNPs synthesized with 10 k PVP.[41,52] These measurement differences are presented in Table 1, which shows a comparison of the mean and mode sizes measured through DLS and NTA for each of the synthesized AuNPs. As can be observed, while all measured sizes are smaller for NTA, measured sizes for 10 k PVP are drastically different between both techniques due to weak stabilization of lower molecular weight PVP towards AuNPs in both the DES and in water.

Plasmonic eutectogel performance

To showcase the stability of the nanoparticles, a proof-of-concept plasmonic eutectogel was explored. The proposed plasmonic eutectogel comprises a gelatin-based eutectogel prepared using the gold colloid in DES as the liquid phase and type A gelatin as the gelator. The formation of the eutectogel is possible due to the gelatin triple helix self-assembly, which occurs through the transition from a sol state, when heated to 90 °C, to a gel state when the sample is cooled overnight at 4 °C.[53]

Fig. S10a† shows that even in a gelling state (eutectogel), the nanoparticles keep their particular purple color. This is a clear indicator that the LSPR of the nanoparticles remains stable (543 nm) and is not affected by the drastic changes in temperatures during the plasmonic eutectogel preparation: from RT, heating to 90 °C, and cooling to 4 °C overnight. The UV-vis spectrum of the solid eutectogel also demonstrates that the LSPR in the eutectogel remains unchanged (Fig. S10b†) even if it was stretched to 100% of its original length at RT, exhibiting the high stability of its optical properties. The LSPR intensity is only affected by the reduction of the length path of the measurement during stretching. The plasmonic eutectogel was characterized by a compression test resulting in an ultimate tensile strength of 2.9 kPa in the first cycle at 50% strain (Fig. 8a), which decreased after the second and third cycles (Fig. S11†). DSC analysis of the eutectogel was also conducted to determine the transition temperature associated with its macroscopic melting. The melting point of the plasmonic eutectogel observed *via* DSC was found to be 40 °C, which is consistent with previously reported values for gelatin-based materials.[53–55] The limited mechanical and thermal properties are inherent to the urea and gelatin-based eutectogel, which can be improved by promoting transient interactions with a favorable DES, *e.g.* ethylene glycol–ChCl DES.[56] Finally, the sensitivity of the eutectogel was calculated according to eqn (1), where the calculated GF was 0.63 (at 150% strain), which is higher than those of other eutectogels based on U–ChCl DES.[57]

 © 2024 The Author(s). Published by the Royal Society of Chemistry

Open Access Article. Published on 12 March 2024. Downloaded on 3/30/2026 8:14:33 AM.
This article is licensed under a Creative Commons Attribution 3.0 Unported Licence.

Table 1 Comparison of the AuNPs' sizes obtained through DLS and NTA techniques

Sample	DLS mean (nm)	NTA mean (nm)	DLS mode (nm)	NTA mode (nm)
10 k	672	172.5	534.4	119.2
40 k	52.5	75.7	68.6	59.5
360 k	126	132.2	169.9	104.5
40 k DES	19.1	—	26.6	—
40 k water	47.5	51.9	43	45.6

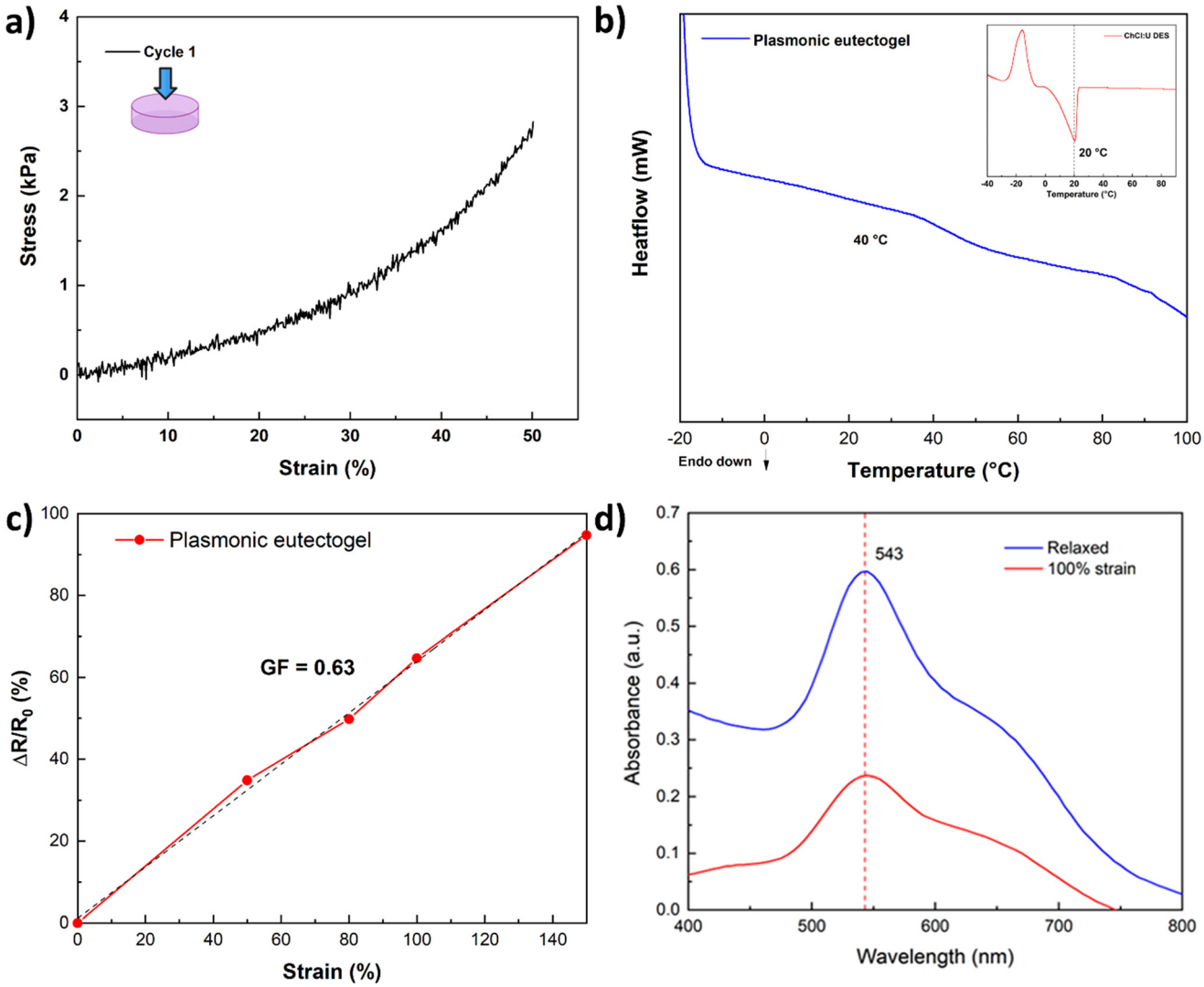

Fig. 8 (a) Compressive stress–strain test and (b) thermogram of the plasmonic aerogel with an inset of the thermogram for U–ChCl DES. (c) Gauge factor (GF) evaluation of the obtained material at 150% strain range and (d) absorption spectra of the relaxed and strained eutectogels obtained through UV-vis spectroscopy.

Conclusions

A systematic investigation into the effect of PVP of varied molecular weights (10, 40 and 360 kDa) on the nonaqueous synthesis of AuNPs in U–ChCl DES was conducted in this work. The synthesis, achieved through chemical reduction with ascorbic acid at 60 °C, resulted in plasmonic AuNPs of *ca.* 20 nm in the case of 40 and 360 k PVP. These syntheses resulted in the formation of quasi spherical-shaped nanoparticles, presenting a characteristic LSPR at around 540 nm, analyzed through UV-vis spectroscopy in the nonaqueous DES. Electron microscopy images indicated that the resulting particle size distributions directly depend on the PVP's M_n, being slightly larger for the AuNPs synthesized with 40 k PVP compared to higher and lower molecular weights, irrespective of the medium viscosity. Multimodal LSPR with peaks at 530 and 810 nm in the gold colloids from 10 k PVP suggested weaker steric stabilization due to the shorter chain length,

Open Access Article. Published on 12 March 2024. Downloaded on 3/30/2026 8:14:33 AM. This article is licensed under a Creative Commons Attribution 3.0 Unported Licence.

making it less effective in confining particle size compared to higher molecular weights. Similar size distributions to 40 k PVP were obtained from the highest M_n, yielding a particle size distribution between 10 and 25 nm and a well-defined spherical morphology. Both the morphology and size distribution resulted from the steric stabilization caused by the high-molecular weight polymer.

PVP with a M_n of 40 kDa demonstrated high effectiveness for AuNP synthesis and stabilization in U–ChCl DES. Interestingly, increasing the PVP concentration in the synthesis led to an increase in the concentration of plasmonic nanoparticles at the expense of fluorescent gold clusters of *ca.* 2 nm. This is attributed to the involvement of PVP as a soft reducing agent. Additionally, the plasmon shape closely resembled that of AuNPs synthesized under the same conditions in aqueous media, establishing the results as a benchmark in the synthesis of shape-controlled nanoparticles in nonaqueous DES with non-toxic capping agents and through a greener route.

Finally, leveraging the remarkable colloidal stability of the nonaqueous gold colloids in DES, a gelatin-based eutectogel was constructed. The resulting plasmonic eutectogel exhibited limited mechanical properties but has a competitive gauge factor as a strain sensor (GF = 0.63) while maintaining the LSPR from the immobilized AuNPs. This work paves the way for dual plasmonic and strain-responsive nonaqueous flexible materials, synthesized with sustainable protocols involving DESs and biopolymers.

Conflicts of interest

There are no conflicts to declare.

Acknowledgements

The authors acknowledge the Laboratorio 14 from the Multidisciplinary Research Unit at FES-Cuautitlan, UNAM for the use of the nanoparticle tracking analysis equipment NanoSight NS300 and zeta potential measurements (Zetasizer Pro-Malvern PANalytical). The authors thank Edgar Franco, Edgar Miranda, and Perla Itzel Alcantara Llanas (CIDESI) for the technical assistance provided in mechanical testing and thermal analysis at the Laboratorio Nacional de Caracterizacion de Materiales (LaNCaM), and Milton Vazquez-Lepe (CUCEI-Universidad de Guadalajara) for the assistance with XPS analysis. The authors acknowledge the financial support from PAPIIT-UNAM projects IN115624 and IA100424.

References

1 E. C. Dreaden, A. M. Alkilany, X. Huang, C. J. Murphy and M. A. El-Sayed, *Chem. Soc. Rev.*, 2012, **41**, 2740–2779.
2 M.-C. Daniel and D. Astruc, *Chem. Rev.*, 2004, **104**, 293–346.
3 Y. Wu, M. R. K. Ali, K. Chen, N. Fang and M. A. El-Sayed, *Nano Today*, 2019, **24**, 120–140.
4 N. Li, P. Zhao and D. Astruc, *Angew. Chem., Int. Ed.*, 2014, **53**, 1756–1789.
5 N. Sarfraz and I. Khan, *Chem. – Asian J.*, 2021, **16**, 720–742.
6 H. Kang, J. T. Buchman, R. S. Rodriguez, H. L. Ring, J. He, K. C. Bantz and C. L. Haynes, *Chem. Rev.*, 2019, **119**, 664–699.
7 Y. Li and R. Jin, *Nanoscale Horiz.*, 2023, **8**, 991–1013.
8 G. A. Vinnacombe-Willson, Y. Conti, A. Stefancu, P. S. Weiss, E. Cortés and L. Scarabelli, *Chem. Rev.*, 2023, **123**, 8488–8529.
9 J. Piella, N. G. Bastús and V. Puntes, *Chem. Mater.*, 2016, **28**, 1066–1075.
10 J. Polte, *CrystEngComm*, 2015, **17**, 6809–6830.
11 A. Heuer-Jungemann, N. Feliu, I. Bakaimi, M. Hamaly, A. Alkilany, I. Chakraborty, A. Masood, M. F. Casula, A. Kostopoulou, E. Oh, K. Susumu, M. H. Stewart, I. L. Medintz, E. Stratakis, W. J. Parak and A. G. Kanaras, *Chem. Rev.*, 2019, **119**, 4819–4880.
12 J. Mosquera, D. Wang, S. Bals and L. M. Liz-Marzán, *Acc. Chem. Res.*, 2023, **56**, 1204–1212.
13 L. Scarabelli, M. Sun, X. Zhuo, S. Yoo, J. E. Millstone, M. R. Jones and L. M. Liz-Marzán, *Chem. Rev.*, 2023, **123**, 3493–3542.
14 J. Zhang, M. R. Langille, M. L. Personick, K. Zhang, S. Li and C. A. Mirkin, *J. Am. Chem. Soc.*, 2010, **132**, 14012–14014.
15 A. S. Barnard, *Acc. Chem. Res.*, 2012, **45**, 1688–1697.
16 Y. Xia, X. Xia and H.-C. Peng, *J. Am. Chem. Soc.*, 2015, **137**, 7947–7966.
17 C. S. Bhatt, A. Rajavel, D. S. Parimi, R. N. Sella, J. Murugaiyan and A. K. Suresh, *ACS Appl. Nano Mater.*, 2023, **6**, 12548–12559.
18 H. Goesmann and C. Feldmann, *Angew. Chem., Int. Ed.*, 2010, **49**, 1362–1395.
19 M. Niederberger, *Adv. Funct. Mater.*, 2017, **27**, 1703647.
20 R. Costi, A. E. Saunders and U. Banin, *Angew. Chem., Int. Ed.*, 2010, **49**, 4878–4897.
21 B. B. Hansen, S. Spittle, B. Chen, D. Poe, Y. Zhang, J. M. Klein, A. Horton, L. Adhikari, T. Zelovich, B. W. Doherty, B. Gurkan, E. J. Maginn, A. Ragauskas, M. Dadmun, T. A. Zawodzinski, G. A. Baker, M. E. Tuckerman, R. F. Savinell and J. R. Sangoro, *Chem. Rev.*, 2021, **121**, 1232–1285.
22 E. L. Smith, A. P. Abbott and K. S. Ryder, *Chem. Rev.*, 2014, **114**, 11060–11082.
23 A. Paiva, R. Craveiro, I. Aroso, M. Martins, R. L. Reis and A. R. C. Duarte, *ACS Sustainable Chem. Eng.*, 2014, **2**, 1063–1071.
24 M. Wysokowski, R. K. Luu, S. Arevalo, E. Khare, W. Stachowiak, M. Niemczak, T. Jesionowski and M. J. Buehler, *Chem. Mater.*, 2023, **35**, 7878–7903.
25 O. S. Hammond and A.-V. Mudring, *Chem. Commun.*, 2022, **58**, 3865–3892.
26 S. Nejrotti, A. Antenucci, C. Pontremoli, L. Gontrani, N. Barbero, M. Carbone and M. Bonomo, *ACS Omega*, 2022, **7**, 47449–47461.
27 L. Adhikari, N. E. Larm and G. A. Baker, *ACS Sustainable Chem. Eng.*, 2020, **8**, 14679–14689.
28 S. Kumar-Krishnan, E. Prokhorov, O. Arias de Fuentes, M. Ramírez, N. Bogdanchikova, I. C. Sanchez, J. D. Mota-Morales and G. Luna-Bárcenas, *J. Mater. Chem. A*, 2015, **3**, 15869–15875.

 © 2024 The Author(s). Published by the Royal Society of Chemistry

Open Access Article. Published on 12 March 2024. Downloaded on 3/30/2026 8:14:33 AM.
This article is licensed under a Creative Commons Attribution 3.0 Unported Licence.

29 S. Datta, J. Mahin, E. Liberti, I. Manasi, K. J. Edler and L. Torrente-Murciano, *ACS Sustainable Chem. Eng.*, 2023, **11**, 10242–10251.
30 R. Seoudi, A. A. Fouda and D. A. Elmenshawy, *Phys. B*, 2010, **405**, 906–911.
31 K. M. Koczkur, S. Mourdikoudis, L. Polavarapu and S. E. Skrabalak, *Dalton Trans.*, 2015, **44**, 17883–17905.
32 L. Sapir, C. B. Stanley and D. Harries, *J. Phys. Chem. A*, 2016, **120**, 3253–3259.
33 M. Luty-Błocho, M. Wojnicki and K. Fitzner, *Int. J. Chem. Kinet.*, 2017, **49**, 789–797.
34 M. H. Hussain, N. F. Abu Bakar, A. N. Mustapa, K.-F. Low, N. H. Othman and F. Adam, *Nanoscale Res. Lett.*, 2020, **15**, 140.
35 H. Liao, Y. Jiang, Z. Zhou, S. Chen and S. Sun, *Angew. Chem., Int. Ed.*, 2008, **47**, 9100–9103.
36 D. M. P. Mingos, in *Gold Clusters, Colloids and Nanoparticles I*, ed. D. M. P. Mingos, Springer International Publishing, Cham, 2014, pp. 1–47.
37 H. Chen, X. Kou, Z. Yang, W. Ni and J. Wang, *Langmuir*, 2008, **24**, 5233–5237.
38 in *Metallopolymer Nanocomposites*, ed. A. D. Pomogailo and V. N. Kestelman, Springer Berlin Heidelberg, Berlin, Heidelberg, 2005, pp. 65–113.
39 M. V. Bandulasena, G. T. Vladisavljević, O. G. Odunmbaku and B. Benyahia, *Chem. Eng. Sci.*, 2017, **171**, 233–243.
40 S. S. Panikar, K. C. Sekhar Reddy, A. L. Gonzalez, G. Ramírez-García, Á. G. Rodríguez, M. A. Mondragon Sosa, P. Salas and J. D. Mota-Morales, *Anal. Chem.*, 2022, **94**, 16470–16480.
41 J. Hou, H. Ci, P. Wang, C. Wang, B. Lv, L. Miao and G. You, *J. Hazard. Mater.*, 2018, **360**, 319–328.
42 L. Panariello, A. N. P. Radhakrishnan, I. Papakonstantinou, I. P. Parkin and A. Gavriilidis, *J. Phys. Chem. C*, 2020, **124**, 27662–27672.
43 M. Wuithschick, A. Birnbaum, S. Witte, M. Sztucki, U. Vainio, N. Pinna, K. Rademann, F. Emmerling, R. Kraehnert and J. Polte, *ACS Nano*, 2015, **9**, 7052–7071.
44 T. Hendel, M. Wuithschick, F. Kettemann, A. Birnbaum, K. Rademann and J. Polte, *Anal. Chem.*, 2014, **86**, 11115–11124.
45 F. S. Mjalli, T. Al-Wahaibi and A. A. Al-Hashmi, *J. Mol. Liq.*, 2015, **206**, 256–261.
46 V. S. Raghuwanshi, M. Ochmann, A. Hoell, F. Polzer and K. Rademann, *Langmuir*, 2014, **30**, 6038–6046.
47 J. Liu, P. N. Duchesne, M. Yu, X. Jiang, X. Ning, R. D. Vinluan III, P. Zhang and J. Zheng, *Angew. Chem., Int. Ed.*, 2016, **55**, 8894–8898.
48 K. Dong, J. Zhou, T. Yang, S. Dai, H. Tan, Y. Chen, H. Pan, J. Chen, B. Audit, S. Zhang and J. Xu, *Appl. Spectrosc.*, 2018, **72**, 1645–1652.
49 L. Kemal, X. C. Jiang, K. Wong and A. B. Yu, *J. Phys. Chem. C*, 2008, **112**, 15656–15664.
50 M. Voronova, N. Rubleva, N. Kochkina, A. Afineevskii, A. Zakharov and O. Surov, *Nanomaterials*, 2018, **8**, 1011.
51 T. Mudalige, H. Qu, D. Van Haute, S. M. Ansar, A. Paredes and T. Ingle, in *Nanomaterials for Food Applications*, ed. A. López Rubio, M. J. Fabra Rovira, M. Martínez Sanz and L. G. Gómez-Mascaraque, Elsevier, 2019, pp. 313–353.
52 A. E. James and J. D. Driskell, *Analyst*, 2013, **138**, 1212–1218.
53 S. Carrasco-Saavedra, N. R. Tanguy, I. García-Nieto, R. Pimentel-Domínguez, M. J. Panzer and J. D. Mota-Morales, *Adv. Mater. Interfaces*, 2024, **11**, 2300536.
54 H. Qin, R. E. Owyeung, S. R. Sonkusale and M. J. Panzer, *J. Mater. Chem. C*, 2019, **7**, 601–608.
55 P. A. Mercadal, M. R. Romero, M. del M. Montesinos, J. P. Real, M. L. Picchio and A. González, *ACS Appl. Electron. Mater.*, 2023, **5**, 2184–2196.
56 J. D. Mota-Morales and E. Morales-Narváez, *Matter*, 2021, **4**, 2141–2162.
57 G. Li, Z. Deng, M. Cai, K. Huang, M. Guo, P. Zhang, X. Hou, Y. Zhang, Y. Wang, Y. Wang, X. Wu and C. F. Guo, *npj Flexible Electron.*, 2021, **5**, 23.